Journal of Sound and Vibration 329 (2010) 3233–3246

Contents lists available at ScienceDirect

Journal of Sound and Vibration

journal homepage: www.elsevier.com/locate/jsvi

Numerical simulation of passive–active cells with microperforated plates or porous veils

A. Bermúdez [a,*], P. Gamallo [b], L. Hervella-Nieto [c], A. Prieto [a,d]

[a] Departamento de Matemática Aplicada, Universidade de Santiago de Compostela, 15782 Santiago de Compostela, Spain
[b] Tecnologías Avanzadas Inspiralia SL, 28034 Madrid, Spain
[c] Departamento de Matemáticas, Universidade da Coruña, 15071 A Coruña, Spain
[d] Applied and Computational Mathematics, California Institute of Technology, MC 217-50, 1200 East California Blvd., CA 91125, USA

ARTICLE INFO

Article history:
Received 29 June 2009
Received in revised form
26 January 2010
Accepted 9 February 2010
Handling Editor: J. Lam
Available online 20 March 2010

ABSTRACT

The main goal of this work consists in the numerical simulation of a multichannel passive–active noise control system based on devices involving a particular kind of cell. Each cell consists of a parallelepipedic box with all their faces rigid, except one of them, where a porous veil or a rigid micro-perforated plate (MPP) is placed. Firstly, the frequency response of a single passive cell is computed, when it is surrounded by an unbounded air domain (an anechoic room) and harmonic excitations are imposed. For the numerical solution of this three-dimensional problem, the original unbounded domain is truncated by using exact perfectly matched layers (PML) and the resulting partial differential equation (PDE) is discretized with a standard finite element method. Secondly, the passive cells are transformed into active by assuming that the opposite face to the passive one may vibrate like a piston in order to reduce noise. The corresponding multichannel active control problem is stated and analyzed in the framework of the optimal control theory. A numerical method is proposed to assess and compare different control configurations.

1. Introduction

An important field of work in many industrial and practical acoustical applications is the design of cells for the control of noise in open or closed enclosures. Obviously, these cells should include some passive method for sound absorption, but it is well known that the use of these kind of methods in the low frequency range is inefficient because large sizes and/or weights of bulky sound-absorbing materials would be required to achieve acceptable performances (see [1]). In contrast, in the last decades active noise control techniques have become very popular thanks to the development of fast digital signal processors (DSP) and because they prove to work well in the low frequency range (see [2]). However, hybrid strategies come from the notion of active absorption in the early fifties in [3], and were later validated experimentally [4].

Concerning the passive control, two different possibilities are considered: a porous veil or a microperforated plate (MPP). Both of them are modelled by means of a surface impedance condition which, in addition to simplify the numerical code, is expected to provide a good performance from the simulation viewpoint in the same way as it does for viscoelastic panels (this was shown in [5]). Acoustic absorbing panels involving MPP systems has been analyzed experimentally in

* Corresponding author.
E-mail addresses: alfredo.bermud@usc.es (A. Bermúdez), pablo.gamallo@itav.es (P. Gamallo), luis.hervella@udc.es (L. Hervella-Nieto), andres.prieto@usc.es, maprieto@acm.caltech.edu (A. Prieto).

0022-460X/$ - see front matter © 2010 Elsevier Ltd. All rights reserved.
doi:10.1016/j.jsv.2010.02.011

Nomenclature

List of symbols

a_j	half of the j-th spatial dimension of the fluid domain
a_j^*	half of the j-th spatial dimension of the computational domain
$\mathbf{b}$	projection vector of the passive observation on the active ones
c	sound speed
$\delta_{\mathbf{a}}$	Dirac's delta supported at point $\mathbf{a}$
$\mathbf{e}_i$	vector of the canonical basis associated to the i-th coordinate
η	fluid viscosity
f	frequency
Γ	porous veil boundary
Γ_0	rigid part of the cell boundary
Γ_D	outer PML boundary
Γ_I	interface boundary between the fluid and the PML domain
Γ_L	inner cell face opposite to the porous veil
Γ_l	rectangular patch corresponding to the l-th loudspeaker
g	volumic acoustic source
γ_j	complex-valued PML coefficient
$\mathbf{I}$	identity matrix
J	cost function
J_n	Bessel function of first kind and order n
N_L	number of loudspeakers
N_S	number of sensors
$\mathbf{n}$	unit outward normal vector on the porous veil face
$\boldsymbol{\nu}$	unit outward normal vector on the rigid cell boundary
ν	control effort weighting factor
Ω	parallelepipedic passive cell
Ω_F	fluid domain
Ω_A	PML domain
ω	angular frequency
p^{in}	pressure field in the interior of the cell
p^{out}	pressure field in the exterior of the cell
ϕ	MPP perforation ratio
r_0	radius of the MPP holes
ρ	fluid mass density
s	MPP thickness
σ_j	PML absorbing function in the j-th Cartesian direction
U_{ad}	convex set of admissible controls
$\mathbf{u}$	vector of control variables
u_l	normal displacement of the l-th speaker
$\mathbf{u}_{\text{op}}$	optimal control vector
$\mathbf{Z}$	transfer matrix of the control problem
x_j	cartesian coordinate in the j-th direction
$\mathbf{x}_j$	spatial coordinates of the j-th sensor
$\mathbf{y}$	vector of particle velocity values at sensor points
Z_0	fluid characteristic impedance
Z_ω	impedance of the porous veil or the MPP
$\mathbf{z}$	pressure observations at sensor points
$\mathbf{z}_0$	passive pressure observations at sensor points
$\mathbf{z}_i$	active pressure observations at sensor points associated to the i-th loudspeaker

Subscripts

h	finite element discretization
M	impedance matching control
R	pressure release control

noise barriers [6], as part of a transparent window system [7], coupled with flexible plates [8] or combining two MPPs with different perforation scale [9]. In all those cases and also in this work, the complex-valued impedance associated to the MPP is based on the Maa's formula (see [10]).

For the cells under study, the sound absorption properties can be improved in the low frequency range by using active control techniques. These techniques are based on the principle of destructive interference and thus restricted to linear systems. The aim is to adjust the total field by tuning a secondary field generated by some actuators and superposed to the primary field (see [2]).

Obviously, the configuration of the active cell, which depends on the scheme to minimize the reflected sound and the geometric position of sensors and loudspeakers, leads to a different cost function in the optimal control problem. More precisely, two different control criteria are stated and analyzed: pressure release (see [11]) and impedance matching (see [12]).

The actuators considered in this paper consists of planar loudspeakers located at the top of the cells whose amplitudes can be adjusted (see Fig. 3); these amplitudes will be the control variables of the active system. The reference sensors, required to provide the error signals, will be placed inside the cell. Such geometrical configuration of the passive–active cells mimics that used in the experimental setup of the passive–active cells done by Cobo et al. in [13–15].

With the purpose of the mathematical modelling of the problem, firstly the equations governing the active cell, i.e. the state equations of the system, are introduced. Secondly, the active control problem corresponding to each criterion is settled in the framework of the theory of optimal control systems governed by partial differential equations (see [16]). In both cases, although the state equation is a partial differential equation, the optimal control problem reduces to a discrete quadratic programming problem due to the fact that the control variable is discrete (a finite set of amplitudes). However, the need of numerical methods for solving the state equation will result in an approximate optimal control problem.

In order to have a method covering a broader range of applications (interior as well as exterior problems), we tackle also the possibility of placing the passive–active cell in an unbounded domain (see [17] for an underwater application of active

control problems in unbounded domains). In this way, the acoustic propagation in large enclosures (airport terminals, train stations, public buildings, etc.) can be simulated numerically and also real experiments performed in anechoic rooms. With this purpose, the problem is stated in an unbounded domain and solved by means of the combination of a perfectly matched layer (PML) and a finite element method (FEM). The PML technique was introduced by Bérenger (see [18]) for electromagnetic wave problems, but it has been soon extended to other fields, such as acoustics, which require also the simulation of wave propagation in unbounded media. Recently, an improvement of PML for Helmholtz equation has been proposed by using unbounded absorbing functions (see [19]). This new PML technique is used in this work.

In summary, the main contribution of this work is to study a numerical simulation methodology for the design and assessment of passive–active cells for noise control. It comprises three main points: (a) the mathematical modelling of porous veils and microperforated plates impinged upon by an arbitrary three-dimensional acoustic pressure field, which extend the current mathematical analysis done in one-dimensional models by using harmonic plane waves with normal or oblique incidence (see for instance [8] or [15]); (b) the numerical simulation of three-dimensional passive–active cells in general geometrical configurations, including both interior and exterior problems, by using a combination of a finite element method and possibly a PML technique; and (c) the numerical evaluation of the noise absorption of the passive–active cells described above, comparing different noise control strategies in a three-dimensional model, where not only the MPP acoustic properties but also the entire geometrical configuration of the cell is taken into account.

The outline of the paper is as follows: in Section 2 the acoustic propagation equations of a single passive cell in an unbounded domain are introduced. In Section 3 a PML technique is used to truncate the unbounded domain. In Section 4 the different active control strategies, based on passive–active cells, are posed in the mathematical framework of the optimal control theory. In Section 5, a finite element method is proposed for solving numerically the state equation and an approximate control problem is established. In Section 6 some numerical results are presented to show the performance of the proposed methodology when applied to real situations. Finally, in Section 7 the capabilities and the possible applications of the implemented numerical method are discussed.

2. The passive cell: statement of the acoustic propagation problem

The system in hand consists of a parallelepipedic passive cell, denoted by Ω, filled with an acoustic fluid (e.g. air). The face of the cell where a porous veil or a MPP is placed is denoted by Γ and the rest of the faces, which are assumed to be rigid, by Γ_0 (see Fig. 1). In what follows, we suppose a harmonic regime of angular frequency ω, a real and positive number. Moreover, it is assumed that there is a noise source acting outside the cell Ω. Since neither the porous veil nor the MPP preserve pressure continuity through the face Γ, the pressure in the interior and in the exterior of Ω will be denoted by p^{in} and p^{out}, respectively.

The source problem for this passive cell is governed by the following mathematical model:

Given an angular frequency $\omega > 0$ and an acoustic source g acting outside the cell Ω, find the pressure fields p^{in} and p^{out} satisfying

$$-\frac{\omega^2}{c^2}p^{\text{in}} - \Delta p^{\text{in}} = 0 \quad \text{in } \Omega, \tag{1}$$

$$-\frac{\omega^2}{c^2}p^{\text{out}} - \Delta p^{\text{out}} = g \quad \text{in } \mathbb{R}^3 \backslash \overline{\Omega}, \tag{2}$$

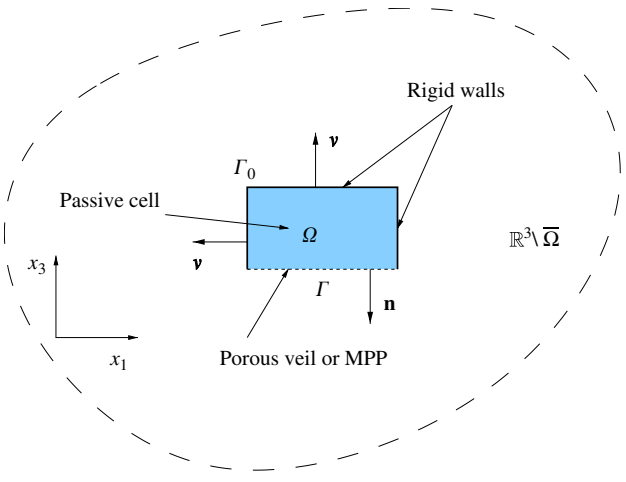

Fig. 1. Vertical cut of the three-dimensional passive cell domain.

$$\frac{\partial p^{\text{in}}}{\partial \mathbf{n}} = \frac{\partial p^{\text{out}}}{\partial \mathbf{n}} \quad \text{on } \Gamma, \tag{3}$$

$$p^{\text{in}} - p^{\text{out}} = Z_\omega \frac{1}{\mathrm{i}\omega\rho} \frac{\partial p^{\text{in}}}{\partial \mathbf{n}} \quad \text{on } \Gamma, \tag{4}$$

$$\frac{\partial p^{\text{in}}}{\partial \boldsymbol{\nu}} = 0, \quad \frac{\partial p^{\text{out}}}{\partial \boldsymbol{\nu}} = 0 \quad \text{on } \Gamma_0, \tag{5}$$

$$\lim_{|\mathbf{x}| = r \to \infty} r\left(\frac{\partial p^{\text{out}}}{\partial r} - \mathrm{i}\frac{\omega}{c} p^{\text{out}}\right) = 0 \quad \text{in } \mathbb{R}^3, \tag{6}$$

where Z_ω is the impedance of the porous veil or the MPP, and $\mathbf{n}$ and $\boldsymbol{\nu}$ are the unit outward normal vectors on Γ and Γ_0, respectively (see Fig. 1).

The proof of the existence and uniqueness of solution to the above problem follows from Fredholm's Alternative (see, for instance, [20]) but it is beyond the scope of this paper.

3. Perfectly matched layer

Let us remark that the computational domain of problem (1)–(6) is unbounded. This is why the Sommerfeld radiation condition (6) has been considered. For numerical solution a PML technique is proposed herein to truncate the unbounded domain (see [18,21]). The PML works as a buffer zone which is designed in a way that any wave entering the PML zone is not reflected and it is damped out when propagating within it.

Let us assume that the cell is contained in the domain

$$\Omega_F = (-a_1, a_1) \times (-a_2, a_2) \times (-a_3, a_3),$$

and focus our attention on computing the pressure field given by (1)–(6) only inside the domain Ω_F. The domain where the absorbing PML layers are located is defined by

$$\Omega_A = \left[(-a_1^*, a_1^*) \times (-a_2^*, a_2^*) \times (-a_3^*, a_3^*)\right] \backslash \overline{\Omega_F},$$

with $a_j < a_j^*$, $1 \le j \le 3$. The set $\Gamma_D = \partial\Omega_A \backslash \Gamma_I$ denotes the exterior boundary of the PML domain (see Fig. 2).

The partial differential equations governing the propagation in the PML can be derived formally by means of a complex-valued change of variable which depends on certain "absorbing" functions σ_j, $j = 1, 2, 3$. This procedure leads to a Helmholtz-like equation with dissipative terms.

Classically, functions σ_j, $j = 1, 2, 3$, are positive, monotonically increasing in the PML, and null in the fluid domain Ω_F. Alternatively, it has been shown in [19] that they can be non-integrable and, in this case, the solution of the original

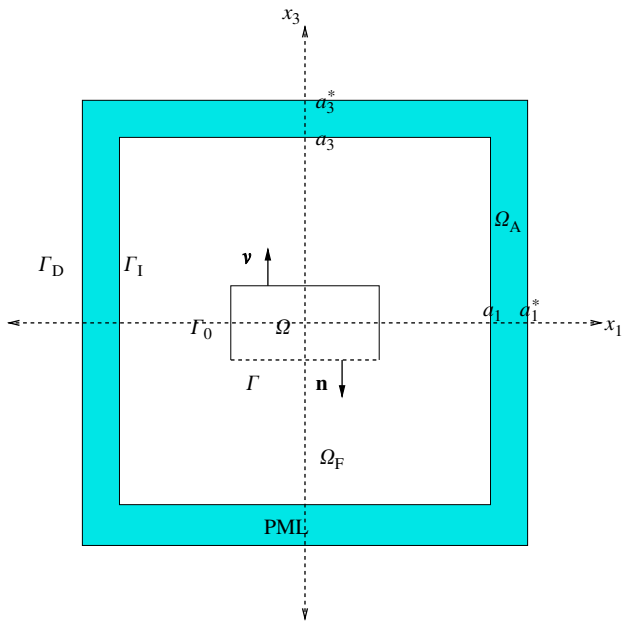

Fig. 2. Vertical cut of the three-dimensional source problem with PMLs.

problem (1)–(6), stated in the original unbounded domain, is recovered exactly in the domain Ω_F even if the PML has finite thickness.

More precisely, let us introduce the following complex-valued coefficients depending on absorbing functions σ_j to be chosen below: $\gamma_j(x_j)=1+\mathrm{i}\sigma_j(x_j)/\omega$, $j=1,2,3$. Then, problem (1)–(6), stated in an unbounded domain, is replaced by the following modified problem in the bounded domain $\Omega_F\cup\Omega_A$:

Given an angular frequency $\omega>0$ and an acoustic source g acting outside Ω, find pressure fields p^{in} and p^{out} satisfying

$$-\frac{\omega^2}{c^2}p^{\mathrm{in}}-\Delta p^{\mathrm{in}}=0 \quad \text{in } \Omega, \tag{7}$$

$$-\frac{\omega^2}{c^2}p^{\mathrm{out}}-\sum_{j=1}^{3}\frac{1}{\gamma_j}\frac{\partial}{\partial x_j}\left[\frac{1}{\gamma_j}\frac{\partial p^{\mathrm{out}}}{\partial x_j}\right]=g \quad \text{in } (\Omega_A\cup\Omega_F)\backslash\overline{\Omega}, \tag{8}$$

$$\frac{\partial p^{\mathrm{in}}}{\partial \mathbf{n}}=\frac{\partial p^{\mathrm{out}}}{\partial \mathbf{n}} \quad \text{on } \Gamma, \tag{9}$$

$$p^{\mathrm{in}}-p^{\mathrm{out}}=Z_\omega\frac{1}{\mathrm{i}\omega\rho}\frac{\partial p^{\mathrm{in}}}{\partial \mathbf{n}} \quad \text{on } \Gamma, \tag{10}$$

$$\frac{\partial p^{\mathrm{in}}}{\partial \boldsymbol{\nu}}=0, \quad \frac{\partial p^{\mathrm{out}}}{\partial \boldsymbol{\nu}}=0 \quad \text{on } \Gamma_0, \tag{11}$$

$$p^{\mathrm{out}}=0 \quad \text{on } \Gamma_D. \tag{12}$$

The key point here is that, by considering suitable non-integrable absorbing functions σ_j, $j=1,2,3$, null in the fluid bounded domain Ω_F, the solutions of problems (1)–(6) and (7)–(12) are exactly the same in Ω_F. This result was rigorously proved for a case with uniform PML layers in polar coordinates, in [22].

4. The passive–active cell: optimal control problem

In this section, going a step further, the passive cell is complemented with an active control system. More precisely, it is assumed that the wall of the cell in front of the porous veil (or the MPP) consists of several patches, each of them vibrating like a piston (planar loudspeaker) so radiating acoustic waves. The aim is to reduce the reflected field by means of the secondary fields generated by the loudspeakers, by adjusting their amplitudes in an appropriate way.

Two different control criteria will be considered in this work: pressure release and impedance matching (see for instance [14]). Note that the extension of the simulation method to other control criteria is straightforward.

4.1. Modelling the passive–active cell

Let us denote by Γ_L the planar face of the parallelepipedic cell opposite to the porous veil (or the MPP). Let us consider a partition of Γ_L consisting of N_L rectangular patches, $\{\Gamma_l\}$, $l=1,\ldots,N_L$, representing the planar loudspeakers (see Fig. 3).

The motion of each loudspeaker is characterized by its normal displacement u_l, $l=1,\ldots,N_L$. Thus, the mathematical model for the acoustic behaviour of the active cell can be written as follows.

Given an angular frequency $\omega>0$ and an acoustic source g acting outside Ω, find pressure fields p^{in} and p^{out} satisfying

$$-\frac{\omega^2}{c^2}p^{\mathrm{in}}-\Delta p^{\mathrm{in}}=0 \quad \text{in } \Omega, \tag{13}$$

$$-\frac{\omega^2}{c^2}p^{\mathrm{out}}-\sum_{j=1}^{3}\frac{1}{\gamma_j}\frac{\partial}{\partial x_j}\left[\frac{1}{\gamma_j}\frac{\partial p^{\mathrm{out}}}{\partial x_j}\right]=g \quad \text{in } \Omega_A\cup\Omega_F, \tag{14}$$

$$\frac{\partial p^{\mathrm{in}}}{\partial \mathbf{n}}=\frac{\partial p^{\mathrm{out}}}{\partial \mathbf{n}} \quad \text{on } \Gamma, \tag{15}$$

$$p^{\mathrm{out}}-p^{\mathrm{in}}=Z_\omega\frac{1}{\mathrm{i}\omega\rho}\frac{\partial p^{\mathrm{in}}}{\partial \mathbf{n}} \quad \text{on } \Gamma, \tag{16}$$

$$\frac{\partial p^{\mathrm{in}}}{\partial \boldsymbol{\nu}}=0 \quad \text{on } \Gamma_0\backslash\Gamma_L, \quad \frac{1}{\mathrm{i}\omega\rho}\frac{\partial p^{\mathrm{in}}}{\partial \boldsymbol{\nu}}=u_l \quad \text{on } \Gamma_l,\ l=1,\ldots,N_L, \tag{17}$$

$$\frac{\partial p^{\mathrm{out}}}{\partial \boldsymbol{\nu}}=0 \quad \text{on } \Gamma_0, \tag{18}$$

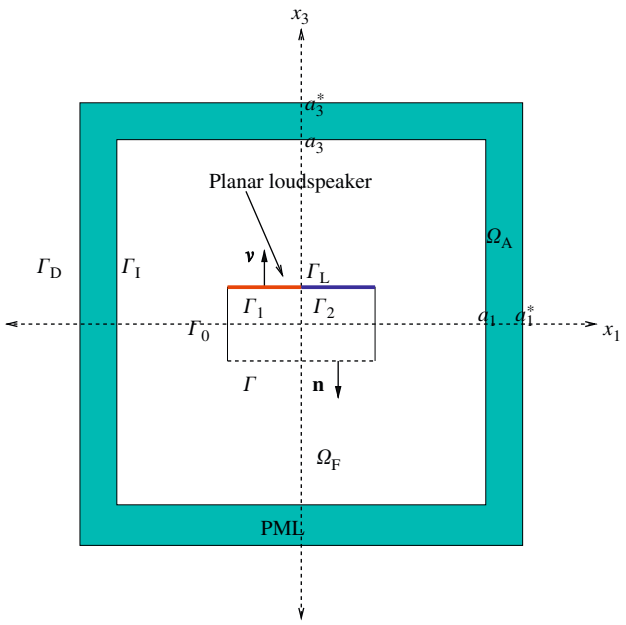

Fig. 3. Vertical cut of the computational domain with the PMLs, corresponding to a three-dimensional source problem with two loudspeakers.

$$p^{\text{out}} = 0 \quad \text{on } \Gamma_D. \tag{19}$$

4.2. Active control techniques: optimal control problems

In this section the active noise control problem is stated as an optimal control problem, in the framework of the theory developed in [16]. It is defined by the following elements:

- Control variable: in the active cell, the normal displacement of each of its N_L loudspeakers can be set freely and therefore the control variable is a complex-valued vector (amplitude and phase) defined by these normal displacements:
$$\mathbf{u} = (u_1, \ldots, u_{N_L}) \in \mathbb{C}^{N_L}.$$
In general, due to technological constraints, the loudspeakers amplitudes are bounded and so they must belong to a convex set of admissible controls $U_{\text{ad}} \subset \mathbb{C}^{N_L}$.
- State of the system: it is given by the pressure fields $(p^{\text{in}}, p^{\text{out}})$ satisfying Eqs. (13)–(19); notice that it depends on the control $\mathbf{u}$.
- Observation: it will be defined, in general, as a linear combination of the pressure and the particle velocity (projected on a certain direction) at N_S sensors placed at points $\mathbf{x}_j$, $j=1,\ldots,N_S$ depending on the control strategy to be used (see below). The particle velocity values will be denoted by $\mathbf{y} \in \mathbb{C}^{N_S}$ and the observations by $\mathbf{z} \in \mathbb{C}^{N_S}$. Notice that, since the state system (13)–(19) is linear, $\mathbf{z}(\mathbf{u})$ will be an affine function of the control $\mathbf{u}$.
- Cost function: it depends on the observation and possibly on the cost of the control itself in the following way:
$$J(\mathbf{u}) := \frac{1}{2}\|\mathbf{z}(\mathbf{u})\|^2 + \frac{\nu}{2}\|\mathbf{u}\|^2,$$
being $\nu \geq 0$ the so-called control effort weighting factor.

Then, the optimal control problem reads as follows:
Find $\mathbf{u}_{\text{op}} \in U_{\text{ad}}$ such that

$$J(\mathbf{u}_{\text{op}}) = \inf_{\mathbf{u} \in U_{\text{ad}}} J(\mathbf{u}). \tag{20}$$

Since the set of admissible controls U_{ad} is a subset of a finite-dimensional space, the mapping between the control and the observation is affine, and the cost function is quadratic with respect to the state and control variables, then the optimal control problem (20) can be written as a discrete quadratic programming problem. This result can be readily proved, as it is shown next. Firstly, let us introduce the primary observation $\mathbf{z}_0$ due to the primary source g (i.e. without active control,

$\mathbf{u}=\mathbf{0}$), and the set of observations

$$\mathbf{z}_i := \mathbf{z}(\mathbf{e}_i),$$

where $\mathbf{e}_i$ denotes the i-th element of the canonical basis in $\mathbb{C}^{N_L}$, namely, $(\mathbf{e}_i)_j = 1$ for $i=j$ and 0 otherwise.

Notice that $\mathbf{z}_i$ corresponds to the observation when the i-th loudspeaker is working with unit amplitude and the rest of them and the primary source g are switched off. Secondly, introducing the transfer matrix $\mathbf{Z} \in \mathbb{C}^{N_L \times N_L}$ and the vector $\mathbf{b} \in \mathbb{C}^{N_L}$ by

$$(\mathbf{Z})_{ij} = (\mathbf{z}_i, \mathbf{z}_j), \quad i,j = 1,\ldots,N_L, \tag{21}$$

$$(\mathbf{b})_i = (\mathbf{z}_0, \mathbf{z}_j), \quad j = 1,\ldots,N_L, \tag{22}$$

where $(\cdot,\cdot)$ is the standard scalar product in $\mathbb{C}^{N_L}$, the observation is given by $\mathbf{z}(\mathbf{u})=\mathbf{Z}\mathbf{u}+\mathbf{b}$. Finally, straightforward calculations show that problem (20) can be written as the following constrained finite-dimensional quadratic programming problem:

Find $\mathbf{u}_{\rm op} \in U_{\rm ad}$ such that

$$J(\mathbf{u}_{\rm op}) = \inf_{\mathbf{u}\in U_{\rm ad}} \left\{ \frac{1}{2}(\mathbf{u},(\mathbf{Z}+\nu\mathbf{I})\mathbf{u}) + (\mathbf{u},\mathbf{b}) + \frac{1}{2}\|\mathbf{z}_0\|^2 \right\}. \tag{23}$$

It can be easily shown that, provided that $\nu > 0$, or $\nu \geq 0$ and $\mathbf{z}(\mathbf{u})$ is an injective mapping, the above optimal control problem has a unique solution (see for instance [23] for a similar problem). Moreover, the optimal control $\mathbf{u}_{\rm op}$ is the solution of the following variational inequality (optimality condition):

$$(\mathbf{v}-\mathbf{u}_{\rm op},(\mathbf{Z}+\nu\mathbf{I})\mathbf{u}_{\rm op}) \geq -(\mathbf{v}-\mathbf{u}_{\rm op},\mathbf{b}) \quad \forall \mathbf{v} \in U_{\rm ad}. \tag{24}$$

When the set of admissible controls $U_{\rm ad}$ is the whole space, i.e., if there are no constraints on the control variable, the above condition reduces to the Euler equation,

$$(\mathbf{Z}+\nu\mathbf{I})\mathbf{u}_{\rm op} = -\mathbf{b}. \tag{25}$$

Let us remark that, if the control effort is null and the number of observation points, N_S, is less or equal than the number of planar loudspeakers, N_L, then $J(\mathbf{u}_{\rm op})=0$, i.e., the pressure field is cancelled at the observation points when the control is optimal.

Two different standard noise control strategies will be analyzed in this work corresponding to two different observations (see [12]):

- Pressure release: the observation to be minimized is the pressure at the center point of the interior side of the porous veil (or the MPP) of each cell; more precisely, it is the scalar

$$\mathbf{z}_{\rm R}(\mathbf{u}) : = (p^{\rm in}(\mathbf{x}_1),\ldots,p^{\rm in}(\mathbf{x}_{N_S})), \tag{26}$$

  so the cost function reads

$$J_{\rm R}(\mathbf{u}) = \frac{1}{2}\sum_{i=1}^{N_S} |p^{\rm in}(\mathbf{x}_i)|^2 + \frac{\nu}{2}\|\mathbf{u}\|^2.$$

- Impedance matching: the goal is that the normal input impedance to the cell matches the characteristic impedance of the medium, Z_0, at the center point of the external side of the porous veil (or the MPP) of each cell. In other words, we want to annulate the observation which corresponds to the i-th cell

$$(\mathbf{z}_M(\mathbf{u}),\mathbf{e}_i) : = p^{\rm out}(\mathbf{x}_i) + Z_0 \frac{1}{{\rm i}\omega\rho}\frac{\partial p^{\rm out}}{\partial \mathbf{n}}(\mathbf{x}_i), \quad i = 1,\ldots,N_S, \tag{27}$$

  by minimizing the cost function

$$J_M(\mathbf{u}) = \frac{1}{2}\|\mathbf{z}_M(\mathbf{u})\|^2 + \frac{\nu}{2}\|\mathbf{u}\|^2. \tag{28}$$

  From a practical point of view, it is preferable to place the error sensor inside the cell rather than outside. For this reason, the observation is obtained indirectly from the pressure and the (normal) particle velocity at the center of the interior side of the porous veil (or the MPP). Thus, taking into account Eqs. (15) and (16) defining the pressure jump across the porous veil (or the MPP), we obtain

$$(\mathbf{z}_M(\mathbf{u}),\mathbf{e}_i) = p^{\rm in}(\mathbf{x}_i) + (Z_0 - Z_\omega)\frac{1}{{\rm i}\omega\rho}\frac{\partial p^{\rm in}}{\partial \mathbf{n}}(\mathbf{x}_i), \quad i = 1,\ldots,N_S.$$

5. Numerical solution: discretization procedure

5.1. Description of the finite element method (FEM)

A standard FEM is used to solve numerically the state equations. Let us consider hexaedral meshes of the two regions, Ω and $(\Omega_F \cup \Omega_A)\backslash\overline{\Omega}$, of the computational domain. Although it is not necessary to have meshes matching on their common interface Γ_I, all the numerical examples below have been performed with compatible meshes. As usual, h denotes the mesh-size. Approximations $p_h^{\rm in}$ and $p_h^{\rm out}$ of $p^{\rm in}$ and $p^{\rm out}$, respectively, are computed by using bilinear hexaedral finite elements. Let us recall that the degrees of freedom defining the finite element solution are the values of $p_h^{\rm in}$ and $p_h^{\rm out}$ at the vertices of the hexaedra.

Regarding the boundary condition on the outer boundaries of the PMLs, a prescribed null pressure is imposed (see Eq. (12)). Hence, $p_h^{\rm out}$ does not have any degrees of freedom on this outer boundary. This condition is essential for the resulting discrete problem to be well posed when non-integrable absorbing functions are used (see [19]).

Let us remark again that, inside the fluid domain Ω_F, the absorbing functions γ_j are equal to one, for $j=1, 2, 3$, because functions σ_j are taken to be null there.

As proposed in [19], in the PML these functions are chosen of the following form:

$$\sigma_j(x_j) = \frac{c}{a_j^* - x_j}, \quad x_j \in [a_j, a_j^*),$$

for $j=1,2,3$. Notice that they are unbounded as x_j goes to a_j^* and also non-integrable in the interval $[a_j, a_j^*)$ corresponding to the j-th PML (see Fig. 3). However, straightforward computations show that the coefficients of the finite element matrices are bounded, in spite of the singularity of σ_j on Γ_D (see [19]).

Let us remark that the complex matrices arising from this finite element discretization, although non-Hermitian, are complex symmetric matrices which allows us to reduce the memory storage when a direct solver is used for solving the linear system. Finally, it is worth mentioning that all the matrix entries have been computed by means of a standard quadrature rule of eight points per hexahedron.

5.2. The discrete optimal control problem

A discrete optimal control problem is obtained when replacing the solution of the original state equation by the FEM approximation of the boundary value problem (13)–(19) involving the PMLs. Let us denote by $(p_h^{\rm in}, p_h^{\rm out})$ the FEM solution corresponding to the mesh size h and by $\mathbf{z}_h(\mathbf{u})$ the corresponding approximation of the observation.

Thus, an approximate cost function is obtained

$$J_h(\mathbf{u}) := \frac{1}{2}\|\mathbf{z}_h(\mathbf{u})\|^2 + \frac{\nu}{2}\|\mathbf{u}\|^2$$

leading to the approximate optimal control problem

$$J_h(\mathbf{u}_{{\rm op}h}) = \inf_{\mathbf{u}\in U_{\rm ad}} J_h(\mathbf{u}). \tag{29}$$

From a mathematical point of view, the above optimal control problem is analogous to the exact one. In particular, a similar inequality to (24), characterizes the approximate optimal control $\mathbf{u}_{{\rm op}h}$, namely

$$(\mathbf{v}-\mathbf{u}_{{\rm op}h}, (\mathbf{Z}_h + \nu\mathbf{I})\mathbf{u}_{{\rm op}h}) \geq -(\mathbf{v}-\mathbf{u}_{{\rm op}h}, \mathbf{b}_h), \quad \forall \mathbf{v} \in U_{\rm ad}. \tag{30}$$

where $\mathbf{Z}_h \in \mathbb{C}^{N_L\times N_L}$ and $\mathbf{b}_h \in \mathbb{C}^{N_L}$ are the approximations of transfer matrix $\mathbf{Z}$ and vector $\mathbf{b}$ given by

$$(\mathbf{Z}_h)_{ij} = (\mathbf{z}_{hi}, \mathbf{z}_{hj}), \quad i,j = 1,\ldots,N_L, \tag{31}$$

$$(\mathbf{b}_h)_j = (\mathbf{z}_{h0}, \mathbf{z}_{hj}), \quad j = 1,\ldots,N_L. \tag{32}$$

In [23,24] it is proven that, provided the matrix $\mathbf{Z}+\nu\mathbf{I}$ is positive definite, i.e., if there exists a positive constant $\alpha > 0$ such that

$$(\mathbf{v}, (\mathbf{Z}+\nu\mathbf{I})\mathbf{v}) \geq \alpha\|\mathbf{v}\|^2, \ \forall \mathbf{v} \in U_{\rm ad},$$

and the mesh size h is small enough, the error of the optimal control is bounded by the error on the transfer matrix and the vector $\mathbf{b}$ through

$$\|\mathbf{u}_{\rm op} - \mathbf{u}_{{\rm op}h}\| \leq \frac{2}{\alpha}\left(\frac{\|\mathbf{b}\|}{\alpha}\|\mathbf{Z}-\mathbf{Z}_h\| + \|\mathbf{b}-\mathbf{b}_h\|\right).$$

Certainly, the error in the observation, and thus the error in the optimal control, will depend on the order of the FEM discretization and the choice of the observation.

6. Numerical results

First, the implementation of numerical method described above is validated by comparing the obtained numerical solution with an explicit exact solution. With this purpose, a normal plane wave propagation problem is chosen.

In order to assess the performance of the passive–active cells introduced in this work for noise control, the acoustic attenuation produced by an isolated cell and surrounded by air is computed. The pressure release and the impedance matching control strategies are taken into account in two different cell configurations. Then, we consider a real-life application where the ceiling of a room is covered with an array of 6×5 passive–active cells.

6.1. Validation

In what follows, the implementation of the numerical method is validated by computing the solution of a normal plane wave propagation problem in the passive case. Let us assume the parallelepipedic computational domain $(-0.75, 0.75) \times (-0.75, 0.75) \times (-0.5, 0.75)$ where all the boundary faces are rigid except those perpendicular to the x_3-axis.

A porous veil is placed at plane $x_3 = 0$ m and a PML domain of thickness 0.25 m is situated between the planes $x_3 = 0.75$ and 0.5 m. The amplitude of the incoming pressure plane wave is fixed to $1\,\mathrm{N/m^2}$, which is imposed on a boundary condition on the face of plane $x_3 = -0.5$ m.

The following physical data are considered: the thickness of the passive fluid cell is 0.15 m and the air properties are $c = 343$ m/s, $\rho = 1\,\mathrm{kg/m^3}$. The complex-valued impedance associated to the porous veil is given by $Z_\omega = Z_0(1-\mathrm{i})\,\mathrm{kg/(m^2\,s)}$.

The exact solution of the previous problem is a plane wave which depends only on the spatial coordinate x_3, i.e.,

$$p(x_3) = \begin{cases} -\dfrac{Z_\omega}{2-Z_\omega} e^{-\mathrm{i}(\omega/c)(x_3+0.5)} + e^{\mathrm{i}(\omega/c)(x_3-0.5)} & \text{if } x_3 \in (-0.5, 0), \\ \dfrac{2}{2-Z_\omega} e^{-\mathrm{i}(\omega/c)(x_3-0.5)} & \text{if } x_3 \in (0, 0.5), \\ \dfrac{x_3+0.75}{0.25} \dfrac{2}{2-Z_\omega} e^{-\mathrm{i}(\omega/c)(x_3-0.5)} & \text{if } x_3 \in [0.5, 0.75). \end{cases}$$

For $f = 100$ Hz and using a uniform finite element mesh with 6137 vertices, the real and imaginary parts of the approximate pressure field has been computed and shown in Fig. 4. In addition, the real and imaginary part of the exact solution are also shown in the same plots with the purpose of comparison.

From these plots it can be verified that: on one hand, the pressure field has a discontinuity at the point where the porous veil is placed; on the other hand, the velocity field, which depends on the derivatives of the pressure field, is continuous. Let us remark that the boundary between the physical and the PML domain is marked with a dash-dot line in both plots.

In order to check the convergence order of the numerical method described in the previous sections, different uniform finite element meshes with 2028, 6137, 13 750, 43 808, and 100 842 vertices have been used to compute the approximate solution. As it is checked in Fig. 5, where the L^2-relative error is plotted versus the mesh-size, the optimal order of convergence is achieved for the piecewise bilinear elements used in the finite element discretization.

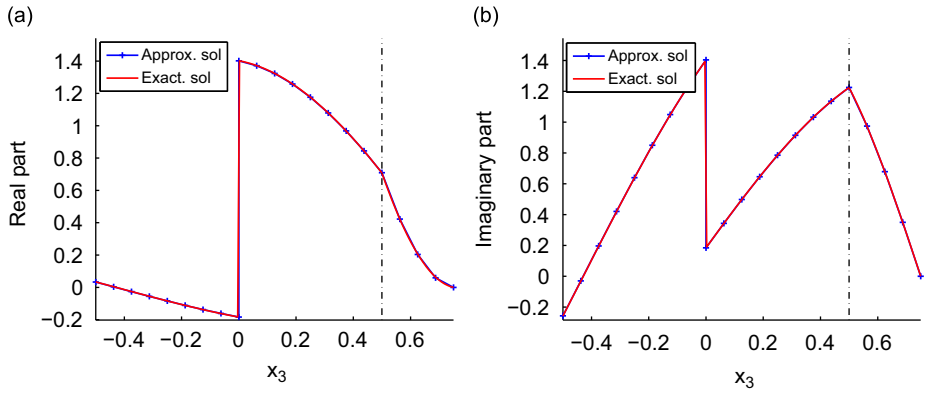

Fig. 4. Plane wave solution for $f = 100$ Hz on line $x_1 = x_2 = 0$: (a) real part, and (b) imaginary part.

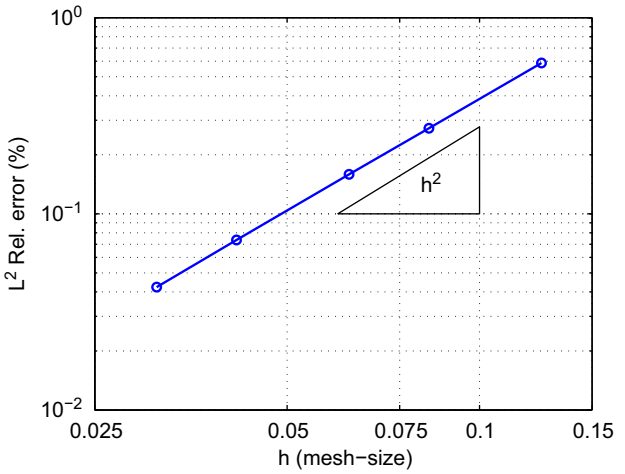

Fig. 5. L^2-relative error (in percentage) computed in the plane wave propagation problem.

6.2. One active cell configuration

In order to determine the impedance associated with the MPP on Γ, the Maa's formula for micro-perforated plates (see [10]) is taken into account, namely

$$Z_\omega = \frac{i\omega\rho s}{\phi}\left(1-\frac{2}{y(\omega)}\frac{J_1(y(\omega))}{J_0(y(\omega))}\right)^{-1}, \tag{33}$$

where s is the thickness of the rigid plate, ϕ the perforation ratio and $y(\omega)=r_0\sqrt{-i\omega\rho/\eta}$, being r_0 the radius of the holes and η the fluid viscosity. $J_n(\cdot)$ is the Bessel functions of first kind and order n.

For the numerical simulations, the following physical data are considered: the size of the passive fluid cell is $0.6\,\text{m}\times 0.6\,\text{m}\times 0.15\,\text{m}$, the air properties are $c=343\,\text{m/s}$, $\rho=1\,\text{kg/m}^3$ and $\eta=1.789\times 10^{-5}\,\text{kg/ms}$. The geometrical data characterizing the MPP are $s=10^{-3}\,\text{m}$, $\phi=0.1$, $r_0=4\times 10^{-3}\,\text{m}$.

Concerning the dimension of the computational domain of interest and the PML domain, we consider the following (in m):

$$\Omega_F=(-0.5,0.5)\times(-0.5,0.5)\times(-0.925,0.925),$$

$$\Omega_A=[(-0.7,0.7)\times(-0.7,0.7)\times(-1.125,1.125)]\backslash\overline{\Omega}_F.$$

To represent the primary field produced by the acoustic source, a pointwise monopole source is located at point $\mathbf{a}=(0,0,-0.725)$ with unitary volume velocity and a complex amplitude depending linearly on the angular frequency and the mass density, i.e., $g=i\omega\rho\delta_{\mathbf{a}}$, where $\delta_{\mathbf{a}}$ is Dirac's delta supported at point $\mathbf{a}$.

Two different configurations have been taken into account. First, a unique loudspeaker is placed covering the back face of the active cell and the pressure observation is done at the inner center point of the porous veil $(0,0,-0.15)$. Second, the original active cell is split into two smaller parts. Each one has a unique loudspeaker as described above. In this case, two observation points are located at $(0,0.17,-0.15)$ and $(0,-0.17,-0.15)$. In both cases a null control effort weighting factor ($v=0$) is assumed.

To compare the pressure level with and without control, the attenuation level is defined by

$$\text{Attenuation (dB)} = 10\log\left(\frac{|p_{\text{op}}|^2}{|p|^2}\right),$$

where p and p_{op} are the computed pressure at the observation point without control and with the optimal control, respectively.

For the pressure release scheme, in Fig. 6 the attenuation fields for the frequencies $f=100$ and $400\,\text{Hz}$ are shown. Analogous graphs for the impedance matching scheme are shown in Fig. 7.

It can be checked from the plots above that, for a frequency of 100 Hz, the attenuation field achieved by the impedance matching strategies reaches $-5\,\text{dB}$ nearby the cell, whereas the pressure release only gets $-3\,\text{dB}$. Moreover, the attenuation field does not show any local maximum in the computational domain at this frequency.

However, if the frequency is fixed to 400 Hz, the attenuation field obtained with both control strategies reaches a reinforcement of 20 dB in a unique centered region with respect to the passive–active cell and a noise attenuation about $-10\,\text{dB}$ with minima periodically distributed in the perpendicular direction to the MPP face of the passive–active cell.

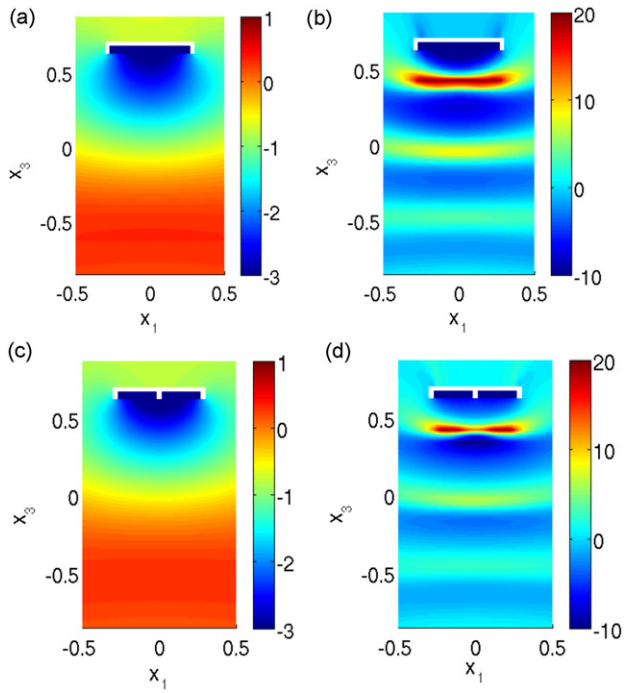

Fig. 6. Pressure release scheme: attenuation field with one sensor and one actuator at 100 and 400 Hz (plots (a) and (b), respectively); attenuation field with two sensors and two actuators at 100 and 400 Hz (plots (c) and (d), respectively).

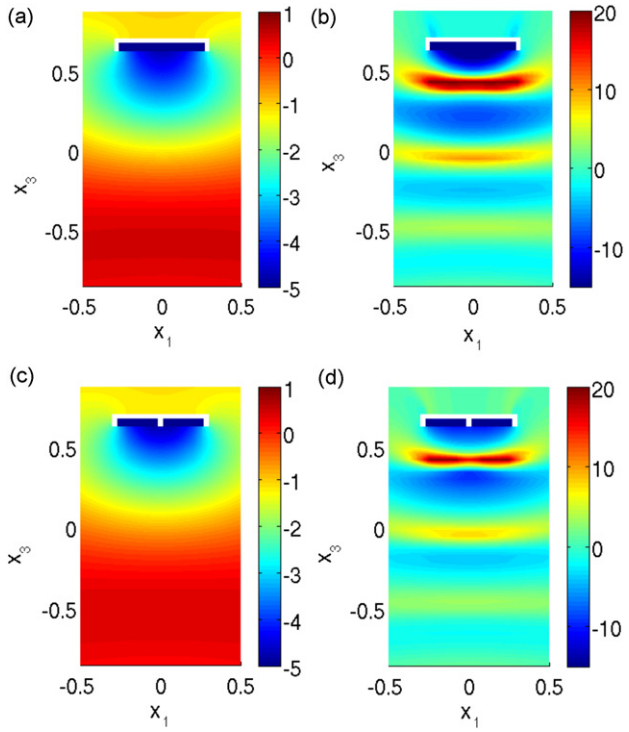

Fig. 7. Impedance matching scheme: attenuation field with one sensor and one actuator at 100 and 400 Hz (plots (a) and (b), respectively); attenuation field with two sensors and two actuators at 100 and 400 Hz (plots (c) and (d), respectively).

Notice that for both frequencies and the two control strategies considered, the one-loudspeaker configuration provides larger attenuation in the neighbourhood of the active cell. Nevertheless, the two-loudspeaker configuration allows us to reduce the area of reinforcement obtained in front of the active cell at 400 Hz.

6.3. Real-life application

Next, the optimal passive–active control of noise in a room whose ceiling has been completely covered with 30 active cells, is computed. The size of each active cell is $0.45\,\mathrm{m} \times 0.45\,\mathrm{m} \times 0.03\,\mathrm{m}$ and they are arranged in an 5×6 array with a separation of 0.05 m among them. The dimensions of the walls, the door and the window of the room are indicated in Fig. 8.

It is worth noting that this problem (or a very similar one) has practical interest and, in fact, it has been the object of previous research, as it can be seen in [25,26].

The door and the window has been modelled by means of impedance boundary conditions. On the one hand, the door is assumed to be open so the classical first-order radiation boundary condition is considered, namely,

$$\frac{\partial p^{\mathrm{out}}}{\partial \mathbf{n}} - \mathrm{i}\frac{\omega}{c} p^{\mathrm{out}} = 0.$$

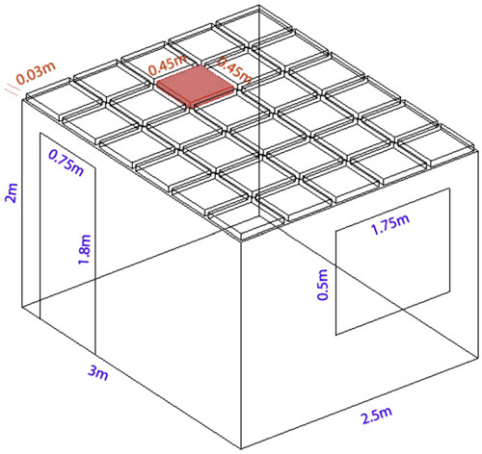

Fig. 8. Three-dimensional geometry of the room with a door (on the left) and a window (on the right).

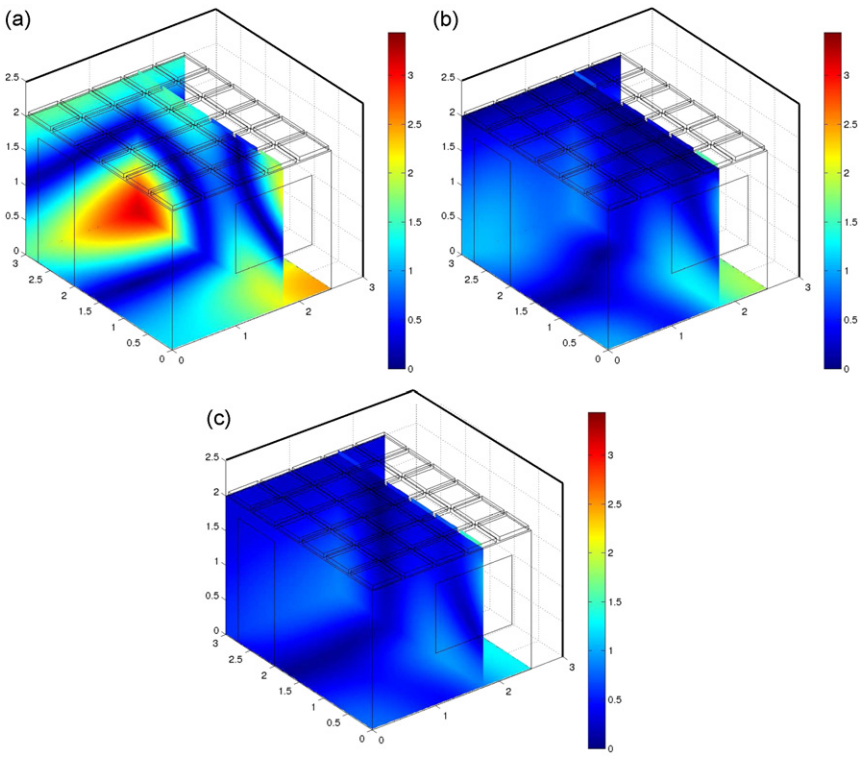

Fig. 9. Amplitude of the pressure field for $f = 100\,\mathrm{Hz}$ for: (a) the passive case, (b) pressure release control, and (c) impedance matching control.

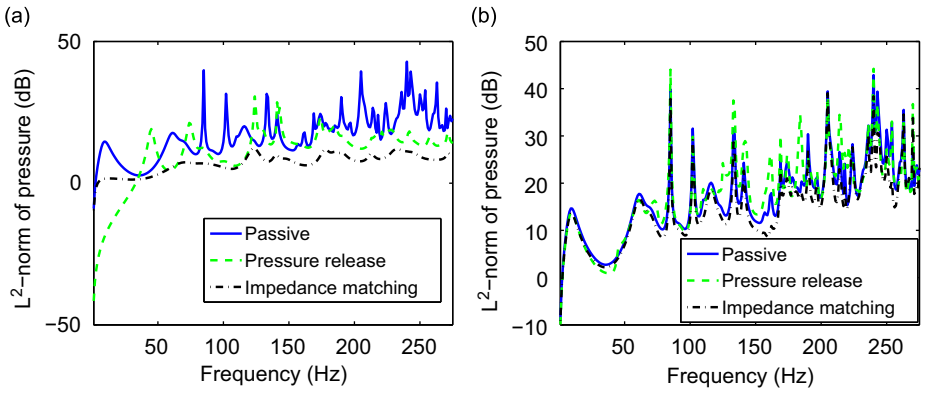

Fig. 10. L^2-norm of pressure (dB) inside the room: (a) with thirty active cells, and (b) with four active cells.

On the other hand, we set a harmonic vibration of unit amplitude incoming through the window (primary field). This has been modelled by the non-homogeneous Robin boundary condition:

$$\frac{\partial p^{\text{out}}}{\partial \mathbf{n}} - \mathrm{i}\frac{\omega}{c} p^{\text{out}} = 1.$$

The remaining walls and the floor are assumed to be rigid, i.e., $\partial p^{\text{out}}/\partial \mathbf{n} = 0$.

For the discretization procedure, a conforming mesh on the cell/room interfaces has been used, with approximately 13×10^3 elements and 86×10^3 degrees of freedom. Let us remark that the motion of each loudspeaker is possibly different in each cell and depends globally on the value of the observations in the cell array.

Fig. 9 shows the modulus of the passive and the active pressure fields, for the cell and the two control strategies described in previous sections taking $f = 100$ Hz. In both strategies, the 30 cells are active. The pressure field has been plotted on planes $x_1 = 1.75$ m, $x_2 = 3$ m, and $x_3 = 0$ m, located inside the room and the active cells.

From the point of view of real-life feasibility of the active control system, it should be guaranteed a uniform pressure level reduction in the low frequency range. Fig. 10 shows the L^2-norm of pressure (in dB) inside the room versus frequency for the different control strategies with 30 active cells.

It can be observed that the pressure norm reduction achieved for the impedance matching control scheme is much more stable for the whole range of frequencies than the pressure release one. However, the latter yields better reduction in the low frequency range between 0 and 40 Hz. Notice that if 30 cells are used with the impedance matching strategy, the reduction of the L^2-norm pressure is pronounced and the peaks corresponding to the resonant frequencies almost vanish.

The performance when only four cells are active is also included on the right-hand side of Fig. 10. In terms of practical implementation, the same four cell configuration has been fixed for the full frequency range. They have been chosen by localizing the four maximal frequency-average of the entries of the transfer matrix. Clearly, despite using any of the active control strategies, the pressure reduction is far from the optimal one computed when 30 cells are active.

7. Conclusions

Two control strategies (pressure release and impedance matching) have been simulated numerically to assess the performance of passive–active cells as sound absorbers. The acoustic effect of a porous veil or a MPP has been included by means of a locally reacting surface impedance model (see [10]).

The discretization procedure for solving the three-dimensional sound propagation model combines a standard FEM and an exact PML technique. The proposed numerical methodology could be used to analyze the performance of potential isolated configurations or the noise absorption of real-life installations as noise barriers [6], absorbers in acoustic window systems [7] or noise reduction devices in flow ducts applications [27].

By using this numerical method, the simulation of a passive–active cell in an anechoic room has been done following as guidance the geometrical setup described in [14]. Overcoming the restrictions that a harmonic plane wave mathematical analysis (at normal or oblique incidence) has, the proposed methodology allows us to evaluate the pressure and attenuation field at any point of the computational domain (see Figs. 6 and 7).

Moreover, the numerical evaluation of the noise absorption of a 6×5 matrix of passive–active cells in a real-life installation has been shown. As it can be checked from the results in the previous section, the proposed methodology based on a finite element code and on the implementation of the active noise reduction problem in the framework of an approximate optimal control problem [16], allows us to evaluate the acoustic attenuation.

Acknowledgements

The work of A. Bermúdez was partially supported by Ministerio de Educación y Ciencia of Spain under Grant MTM2008-02483 and Xunta de Galicia Grant 2006/98.

The work of P. Gamallo was partially supported by Ministerio de Educación y Ciencia of Spain under Grants MTM2008-02483 and 18-08-463B-750, and by Xunta de Galicia under Grant PGIDIT07PXIB105257PR.

The work of L. Hervella-Nieto was partially supported by Ministerio de Educación y Ciencia of Spain under Grants MTM2008-02483 and MTM2007-67596-C02-01 and by Xunta de Galicia under Grant PGIDIT07PXIB105257PR.

The work of A. Prieto was partially supported by Ministerio de Educación y Ciencia of Spain under Grant MTM2008-02483 and by Xunta de Galicia under Grant PGIDIT07PXIB105257PR and program Angeles Alvariño 2007/AA-076.

References

[1] L.L. Beranek, I.L. Vér (Eds.), *Noise and vibration control engineering: principles and applications*, John Wiley & Sons, Hoboken, New Jersey, 2006.
[2] P.A. Nelson, S.J. Elliot, *Active Control of Sound*, Academic Press, New York, 1992.
[3] H.F. Olson, E.G. May, Electronic sound absorber, *Journal of the Acoustical Society of America* 25 (6) (1953) 1130–1136.
[4] D. Guicking, E. Lorenz, An active sound absorber with porous plate, *Journal of Vibration and Acoustics* 106 (3) (1984) 389–392.
[5] A. Bermúdez, L.M. Hervella-Nieto, A. Prieto, R. Rodríguez, Validation of acoustic models for time-harmonic dissipative scattering problems, *Journal of Computational Acoustics* 15 (1) (2007) 95–121.
[6] F. Asdrubali, G. Pispola, Properties of transparent sound-absorbing panels for use in noise barriers, *Journal of the Acoustical Society of America* 121 (1) (2007) 214–221.
[7] J. Kang, M.W. Brocklesby, Feasibility of applying micro-perforated absorbers in acoustic window systems, *Applied Acoustics* 66 (6) (2005) 669–689.
[8] T. Dupont, G. Pavic, B. Laulagnet, Acoustic properties of lightweight micro-perforated plate systems, *Acta Acustica united with Acustica* 28 (2) (2003) 201–212.
[9] J. Pfretzschner, P. Cobo, F. Simón, M. Cuesta, A. Fernández, Microperforated insertion units: an alternative strategy to design microperforated panels, *Applied Acoustics* 67 (1) (2006) 62–73.
[10] D.Y. Maa, Microperforated-panel wideband absorbers, *Noise Control Engineering Journal* 29 (3) (1987) 77–84.
[11] M. Furstoss, D. Thenail, M.A. Galland, Surface impedance control for sound absorption: direct and hybrid passive/active strategies, *Journal of Sound and Vibration* 203 (2) (1997) 219–236.
[12] S. Beyene, R.A. Burdisso, A new hybrid passive–active noise absorption system, *Journal of the Acoustical Society of America* 101 (3) (1997) 1512–1515.
[13] P. Cobo, J. Pfretzschner, M. Cuesta, D.K. Anthony, Hybrid passive–active absorption using microperforated panels, *Journal of the Acoustical Society of America* 116 (4) (2004) 2118–2125.
[14] P. Cobo, A. Fernández, Hybrid passive–active absorption of broadband noise using MPPs, *Noise & Vibration Worldwide* 37 (5) (2006) 19–23.
[15] P. Cobo, M. Cuesta, Measuring hybrid passive–active sound absorption of a microperforates liner at oblique incidence, *Journal of the Acoustical Society of America* 125 (1) (2009) 185–190.
[16] J.L. Lions, *Optimal Control of Systems Governed by Partial Differential Equations*, Springer-Verlag, Berlin, 1971.
[17] Z. Zhang, Y. Chen, X. Yin, H. Hua, Active vibration isolation and underwater sound radiation control, *Journal of Sound and Vibration* 318 (4–5) (2008) 725–736.
[18] J.P. Berenger, A perfectly matched layer for the absorption of electromagnetic waves, *Journal of Computational Physics* 114 (2) (1994) 185–200.
[19] A. Bermúdez, L.M. Hervella-Nieto, A. Prieto, R. Rodríguez, An optimal perfectly matched layer with unbounded absorbing function for time-harmonic acoustic scattering problems, *Journal of Computational Physics* 223 (2) (2007) 469–488.
[20] J.C. Nedelec, *Acoustic and Electromagnetic Equations: Integral Representations for Harmonic Problems*, Springer, New York, 2001.
[21] A. Bermúdez, L.M. Hervella-Nieto, A. Prieto, R. Rodríguez, Perfectly matched layers, in: S. Marburg, B. Nolte (Eds.), *Computational Acoustics of Noise Propagation in Fluids*, Springer-Verlag, Berlin, Heidelberg, 2008, pp. 167–196 (Chapter 6).
[22] A. Bermúdez, L.M. Hervella-Nieto, A. Prieto, R. Rodríguez, An exact bounded perfectly matched layer for time-harmonic scattering problems, *SIAM Journal on Scientific Computing* 30 (1) (2007/2008) 312–338.
[23] A. Bermúdez, P. Gamallo, R. Rodríguez, Finite element methods in local active control of sound, *SIAM Journal on Control and Optimization* 43 (2) (2004) 437–465.
[24] P. Gamallo, Contribución al estudio matemático de problemas de simulación elastoacústica y control activo del ruido, Contribution to the mathematical study of elastoacoustic simulation and active control of sound problems, Ph.D. Thesis, University of Santiago de Compostela, 2002 (in Spanish).
[25] M. Tarabini, A. Roure, Modeling of influencing parameters in active noise control on an enclosure wall, *Journal of Sound and Vibration* 311 (3–5) (2008) 1325–1339.
[26] M. Tarabini, A. Roure, C. Pinhede, Active control of noise on the source side of a partition to increase its sound isolation, *Journal of Sound and Vibration* 320 (4–5) (2009) 726–743.
[27] N. Sellen, M. Cuesta, M.-A. Galland, Noise reduction in a flow duct: implementation of a hybrid passive/active solution, *Journal of Sound and Vibration* 297 (3–5) (2006) 492–511.